Hindawi Publishing Corporation
EURASIP Journal on Advances in Signal Processing
Volume 2008, Article ID 283483, 8 pages
doi:10.1155/2008/283483

Research Article

Multitarget Identification and Localization Using Bistatic MIMO Radar Systems

Haidong Yan, Jun Li, and Guisheng Liao

National Lab of Radar Signal Processing, Xidian University, Xi'an 710071, China

Correspondence should be addressed to Jun Li, junli01@mail.xidian.edu.cn

Received 19 April 2007; Revised 19 September 2007; Accepted 12 November 2007

Recommended by Arden Huang

A scheme for multitarget identification and localization using bistatic MIMO radar systems is proposed. Multitarget can be distinguished by Capon method, as well as the targets angles with respect to transmitter and receiver can be synthesized using the received signals. Thus, the locations of the multiple targets are obtained and spatial synchronization problem in traditional bistatic radars is avoided. The maximum number of targets that can be uniquely identified by proposed method is also analyzed. It is indicated that the product of the numbers of receive and transmit elements minus-one targets can be identified by exploiting the fluctuating of the radar cross section (RCS) of the targets. Cramer-Rao bounds (CRB) are derived to obtain more insights of this scheme. Simulation results demonstrate the performances of the proposed method using Swerling II target model in various scenarios.

1. INTRODUCTION

Multiple-input multiple-output (MIMO) radar has been recently become a hot research area for its potential advantages. MIMO radar uses multiple antennas to simultaneously transmit several independent waveforms and exploit multiple antennas to receive the reflected signals. The echo signals are independent of each other [1–7]. Unlike conventional phased-array radar, MIMO radar systems transmit different signals from different transmit elements. Thus, the whole space can be covered by the electromagnetic waves which are transmitted by the transmit array. Recently, many MIMO radar schemes have been proposed to resist the fluctuations of the target radar cross section (RCS) with the spatial diversity of target scatters to get superiority with waveform diversity in MIMO radar [1], to improve detection performance [2], to create spatial beampatterns ranging from the high directionality of phased-array system to the omnidirectionallity of MIMO system with orthogonal signals through the choice of a signal cross-correlation matrix [3], or to achieve high resolution and excellent interference rejection capability with the direct application of many adaptive techniques [4]. In [5, 6], additional array freedom and super-resolution processing have been achieved by exploiting virtual array sensors in monostatic MIMO radar system. The synthetic impulse and aperture radar (SIAR) is also a monostatic MIMO radar scheme [8]. In conventional bistatic radar, it is required that the transmitting beam and the receiving beam illuminate to the same target simultaneously to solve space synchronization problem [9]. A bistatic MIMO radar scheme of transmit spatial diversity had been proposed in [7], and the estimation performance is analyzed. However, only the angles with respect to the receiver can be determined in this scheme.

A bistatic MIMO radar scheme is proposed to identify and locate multiple targets in this paper. Two-dimensional spatial spectrum estimation is carried out at the receiver. Specially, the method proposed in this paper can parry automatically the spatial 2D angles of targets, which solves the space synchronization problem in conventional bistatic radar system. Maximum number of targets that can be uniquely identified by proposed method is also analyzed in this paper. It is indicated that the product of the number of receive and transmit elements minus-one targets can be identified in the case of independently distributed targets by exploiting the uncorrelation of the reflection coefficients of the targets. Our scheme can be viewed as an extension of the scheme in [5, 10].

This paper is organized as follows. The bistatic MIMO radar signal model is presented in Section 2. In Section 3, the sufficient statistic and the Capon estimator for identification

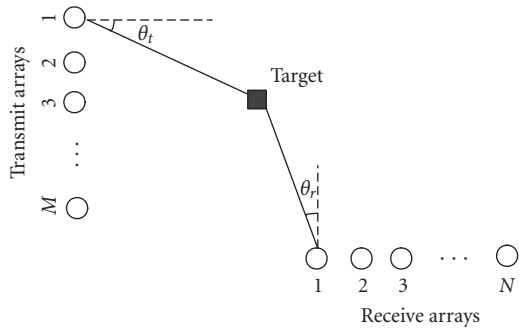

Figure 1: Bistatic MIMO radar scenario.

and location are proposed. The maximum number of identified targets and Cramer-Rao bounds (CRB) for target location are analyzed in Section 4 to obtain more insights of the proposed scheme. The proposed scheme is tested via a few cases and simulations, which appear in Section 5. Finally, Section 6 concludes the paper.

2. BISTATIC MIMO RADAR SIGNAL MODEL

The array structure used in this paper is illustrated in Figure 1. For clarity and mathematical tractability, we use a simple model that ignores Doppler effects and clutters, and the range of the target is assumed much larger than the aperture of transmit array and receive array. Considering the RCS which is constant during a pulse period and varying independently pulse to pulse, our target model is a classical Swerling Case II [11]. The transmit and receive arrays are uniform linear arrays (ULA) with M elements at the transmitter and N elements at the receiver. The elements at the transmitter are omnidirectional. d_t is the interelement space at the transmitter and d_r is the interelement space at the receiver. Assume that the target is at angles (θ_t,θ_r), where θ_t is the angle of the target with respect to the transmit array and θ_r is the angle with respect to the receive array. λ denotes the carrier wavelength. $\mathbf{s}_i = [s_i(1),\ldots,s_i(L)]^T$, $i = 1\cdots M$, denotes the coded pulse of the ith transmitter, where L represents the number of codes in one pulse period. In the case of a single target at location (θ_t,θ_r), the received signal vector of one pulse period is given by

$$\mathbf{r}(n) = \alpha\mathbf{a}(\theta_r)\mathbf{b}^T(\theta_t)\mathbf{S}(n) + \mathbf{w}(n), \tag{1}$$

where $(\cdot)^T$ denotes the vector/matrix transpose. $\mathbf{r}(n) = [r_1(n)\ r_2(n)\ \cdots\ r_2(n)]^T$, $\mathbf{S}(n) = [s_1(n)\ s_2(n)\ \cdots\ s_M(n)]^T$ with $n = 1\cdots L$. α denotes the coefficient involving the reflection coefficients and path loses of the target and we call it reflection coefficient for short in this paper. $\mathbf{a}(\theta_r) = [1\ e^{j(2\pi/\lambda)d_r\sin\theta_r}\ e^{j(2\pi/\lambda)2d_r\sin\theta_r}\ \cdots\ e^{j(2\pi/\lambda)(N-1)d_r\sin\theta_r}]^T$ is an $N\times 1$ vector, usually referred to as the receiver steering vector. $\mathbf{b}(\theta_r) = [1\ e^{j(2\pi/\lambda)d_t\sin\theta_t}\ e^{j(2\pi/\lambda)2d_t\sin\theta_t}\ \cdots\ e^{j(2\pi/\lambda)(M-1)d_t\sin\theta_t}]^T$ is an $M\times 1$ vector, which is usually described as the transmitter steering vector. The noise vectors $\{w(n)\}_{n=1}^N$ are assumed to be independent, zero-mean complex Gaussian distribution with $\mathbf{w}\sim N^c(0,\sigma_w^2\mathbf{I}_N)$.

In the case of P targets, (1) is modified to

$$\mathbf{r}(n) = \mathbf{A}(\theta_r)\mathrm{diag}(\boldsymbol{\alpha})\mathbf{B}^T(\theta_t)\mathbf{S}(n) + \mathbf{w}(n), \tag{2}$$

where $\mathbf{A}(\theta_r) = [\mathbf{a}(\theta_{r_1})\ \mathbf{a}(\theta_{r_2})\ \cdots\ \mathbf{a}(\theta_{r_p})]$ is the receive steering matrix, and $\theta_{r_1}\cdots\theta_{r_p}$ denote the angles of the targets with respect to the receive array. $\mathbf{B}(\theta_t) = [\mathbf{b}(\theta_{t_1})\ \mathbf{b}(\theta_{t_2})\ \cdots\ \mathbf{b}(\theta_{t_p})]$ is the transmit steering matrix, and $\theta_{t_1}\cdots\theta_{t_p}$ denote the angles of the targets with respect to the transmit array. diag($\mathbf{v}$) denotes a diagonal matrix constructed by the vector $\mathbf{v}$. $\boldsymbol{\alpha} = [\alpha_1\cdots\alpha_p]^T$, where $\alpha_1\cdots\alpha_p$ are the reflection coefficients of each target.

3. CAPON-BASED TARGETS IDENTIFICATION AND LOCATION

For simplicity, we assume first that there is only one target in the space and the signal of one pulse period is transmitted from each transmit element. For orthogonal-transmitted waveforms such that $\mathbf{s}_i\mathbf{s}^*{}_j = 0$, $\mathbf{s}_i\mathbf{s}_i = |\mathbf{s}_i|^2$ $i\neq j = 1\cdots M$, where $\mathbf{s}_i$, $\mathbf{s}_j$ stand for the signals transmitted from the ith and jth transmit elements. The received signal $\mathbf{r}(n)$ can be matched by the transmitted waveform to yield a sufficient static matrix as follows:

$$\mathbf{Y} = \frac{1}{L}\sum_{n=1}^{L}\mathbf{r}(n)\mathbf{S}(n)^H, \tag{3}$$

where $(\cdot)^H$ denotes the Hermitian operation.

Substitution of (1) into (3), the independent sufficient statistic vector can be expressed as

$$\begin{aligned}
\boldsymbol{\eta} &= \mathrm{row}(\mathbf{Y}) = \mathrm{row}\left(\frac{1}{L}\sum_{n=1}^{L}\mathbf{r}(n)\mathbf{S}(n)^H\right)\\
&= \mathrm{row}\left(\frac{1}{L}\left(\sum_{n=1}^{L}\alpha\mathbf{a}(\theta_r)\mathbf{b}^T(\theta_t)\mathbf{S}(n)\mathbf{S}^H(n) + \mathbf{w}(n)\mathbf{S}^H(n)\right)\right)\\
&= \mathrm{row}\left(\alpha\sum_{n=\mathbf{1}}^{L}\mathbf{a}(\theta_r)\mathbf{b}^T(\theta_t)\frac{1}{L}\mathbf{S}(n)\mathbf{S}^H(n) + \frac{1}{L}\sum_{n=1}^{L}\mathbf{w}(n)\mathbf{S}^H(n)\right)\\
&= \mathrm{row}(\alpha\mathbf{a}(\theta_r)\mathbf{b}^T(\theta_t)\mathbf{R}_s) + \mathrm{row}\left(\frac{1}{L}\sum_{n=1}^{L}\mathbf{w}(n)\mathbf{S}^H(n)\right)\\
&= \alpha\boldsymbol{\kappa}(\theta_r,\theta_t) + \mathbf{v},
\end{aligned} \tag{4}$$

where $\mathbf{R}_s = (1/L)\sum_{n=1}^{L}\mathbf{S}(n)\mathbf{S}^H(n)$, and $\mathbf{R}_s$ is the identify matrix when transmitted signals are orthogonal. $\boldsymbol{\kappa}(\theta_r,\theta_t) = \mathrm{row}(\mathbf{a}(\theta_r)\mathbf{b}^T(\theta_t)\mathbf{R}_s) = \mathrm{row}(\mathbf{a}(\theta_r)\mathbf{b}^T(\theta_t))$ is a vector with the size of $MN\times 1$ and $\mathbf{v} = \mathrm{row}((1/L)\sum_{n=1}^{L}\mathbf{w}(n)\mathbf{S}^H(n))$ is zero-mean complex Gaussian with $\mathbf{v}\sim N^c(0,\sigma_w^2\mathbf{I}_{NM})$. row$(\cdot)$ denotes the operator that stacks the rows of a matrix in a column vector.

When the number of the targets is P and the signals of Q pulses period are transmitted, (4) can be expressed as follows:

$$\mathbf{Y}_\eta = \mathbf{K}(\theta_r,\theta_t)\mathbf{H} + \mathbf{v}, \tag{5}$$

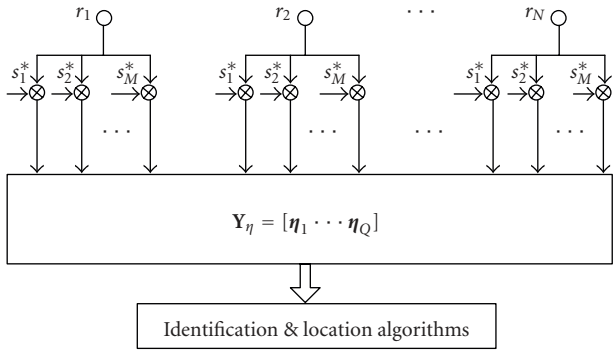

Figure 2: Sufficient statistic extraction and identification and localization algorithms.

where $\mathbf{Y}_\eta = [\boldsymbol{\eta}_1 \cdots \boldsymbol{\eta}_Q]$, and $\boldsymbol{\eta}_1 \cdots \boldsymbol{\eta}_Q$ are the sufficient statistic vectors obtained from Q transmitting pulses. $\mathbf{K}(\theta_r, \theta_t) = [\boldsymbol{\kappa}(\theta_{r_1}, \theta_{t_1}) \cdots \boldsymbol{\kappa}(\theta_{r_p}, \theta_{t_p})]$ is a matrix of size $MN \times P$,

$$\mathbf{H} = \begin{bmatrix} \alpha_{11} & \alpha_{12} & \cdots & \alpha_{1Q} \\ \alpha_{21} & \alpha_{22} & \cdots & \alpha_{2Q} \\ \vdots & \vdots & \ddots & \vdots \\ \alpha_{P1} & \alpha_{P2} & \cdots & \alpha_{PQ} \end{bmatrix}_{P\times Q} \tag{6}$$

where α_{ij}, $i = 1 \cdots P$, $j = 1 \cdots Q$ is the reflection coefficient of the ith target in the jth transmit pulse period. The configuration for obtaining the sufficient static from the data is described in Figure 2.

In practice, different targets have different reflections and path losses. Considering Swerling Case II target model [11], we assume that α_i obeys the complex Gaussian distribution with zero mean and variance $\sigma_{\alpha_i}^2$, namely $\alpha_i \sim {}^c(0, \sigma_{\alpha_i}^2)$, $i = 1 \cdots P$. The Capon estimator [12] of θ_t, θ_r can be written in the form

$$P_{\text{Capon}}(\hat{\theta}_t, \hat{\theta}_r) = \frac{1}{\boldsymbol{\kappa}^H(\theta_r, \theta_t)\mathbf{R}_\eta^{-1}\boldsymbol{\kappa}(\theta_r, \theta_t)}, \tag{7}$$

where $\mathbf{R}_\eta = (1/Q)\mathbf{Y}_\eta\mathbf{Y}_\eta^H$.

The true targets locations will result in the peaks at the Capon estimator outputs.

4. PROPERTY ANALYSIS

4.1. Maximum number of target analysis

From (5), the coherence matrix $\mathbf{R}_\eta$ can be expressed as

$$\mathbf{R}_\eta = \frac{1}{Q}\mathbf{Y}_\eta\mathbf{Y}_\eta^H = \mathbf{K}(\theta_r, \theta_t)\mathbf{R}_H\mathbf{K}^H(\theta_r, \theta_t) + \sigma_w^2\mathbf{I}_{NM}, \tag{8}$$

where $\mathbf{R}_H = (1/Q)\mathbf{H}\mathbf{H}^H$. We can configure the array structure to ensure the column full rank of $\mathbf{K}(\theta_r, \theta_t)$. If $\mathbf{K}(\theta_r, \theta_t)$ is column full rank, the maximum number of targets that can be identified depends on the rank of $\mathbf{R}_\eta$. It is clear that the maximum rank of $\mathbf{R}_\eta$ is NM. So the maximum number of the targets that can be identified by this scheme is $(NM - 1)$.

To ensure the maximum number of targets identification, the matrix $\mathbf{R}_H$ should be full rank. The uncorrelation of the targets reflection coefficients may guarantee the full rank of $\mathbf{R}_H$. Accordingly, the maximum number of identification should be achieved by making use of the uncorrelation of the reflection coefficients of the targets. Our target model in the simulations of the next section is a classical Swerling case II with RCS fluctuations fixing during a transmitting pulse and varying independently pulse to pulse. The targets which are assumed independent of each other in the space and the reflection coefficients of different targets are independent in one pulse period.

4.2. Cramer-Rao bound

Following the approach in [13, Chapter 3] and [14], the stochastic CRB for location parameters of multiple targets is calculated here to obtain more insights of the proposed scheme. The Fisher information matrix (FIM) can be calculated as follows:

$$\begin{aligned} \mathbf{J}(\boldsymbol{\xi}) &= \frac{1}{2}\text{tr}\left[\mathbf{R}_\eta^{-1}(\boldsymbol{\xi})\frac{\partial \mathbf{R}_\eta(\boldsymbol{\xi})}{\partial \boldsymbol{\xi}}\mathbf{R}_\eta^{-1}(\boldsymbol{\xi})\frac{\partial \mathbf{R}_\eta(\boldsymbol{\xi})}{\partial \boldsymbol{\xi}}\right] \\ &= \begin{bmatrix} \mathbf{J}_{\theta_r\theta_r} & \mathbf{J}_{\theta_r\theta_t} & \mathbf{J}_{\theta_r\sigma_\alpha} & \mathbf{J}_{\theta_r\sigma_w} \\ \mathbf{J}_{\theta_r\theta_t}^T & \mathbf{J}_{\theta_t\theta_t} & \mathbf{J}_{\theta_t\sigma_\alpha} & \mathbf{J}_{\theta_t\sigma_w} \\ \mathbf{J}_{\theta_r\sigma_\alpha}^T & \mathbf{J}_{\theta_t\sigma_\alpha}^T & \mathbf{J}_{\sigma_\alpha\sigma_\alpha} & \mathbf{J}_{\sigma_\alpha\sigma_w} \\ \mathbf{J}_{\theta_r\sigma_w}^T & \mathbf{J}_{\theta_t\sigma_w}^T & \mathbf{J}_{\sigma_\alpha\sigma_w}^T & \mathbf{J}_{\sigma_w\sigma_w} \end{bmatrix}, \end{aligned} \tag{9}$$

where $\boldsymbol{\xi} = [\boldsymbol{\theta}_r^T\boldsymbol{\theta}_t^T\boldsymbol{\sigma}_\alpha\sigma_w]^T$ and $\boldsymbol{\sigma}_\alpha = [\sigma_{\alpha_1} \cdots \sigma_{\alpha_p}]^T$. The derivation of the submatrices of FIM in (9) is given in the appendix. We can calculate the variance of an individual estimated parameter by inverting the FIM, namely,

$$\mathbf{CRB}(\boldsymbol{\xi}) = \text{diag}(\mathbf{J}^{-1}(\boldsymbol{\xi})), \tag{10}$$

where $\text{diag}(\cdot)$ denotes a vector constructed by the diagonal elements of the matrix $(\cdot)$.

In (10), the first P elements of $\mathbf{CRB}(\boldsymbol{\xi})$ are the CRB for $\theta_{r_1} \cdots \theta_{r_p}$ and the second P elements are the ones for $\theta_{t_1} \cdots \theta_{t_p}$.

4.3. Analysis of the CRB

The transmit signals used in this subsection are as follows.

Hadamard code pulse signals (HCP): each transmitter transmits the different Hadamard code with the same carrier frequency.

The step-frequency Hadamard code pulse signals (FHCP): each transmitter transmits different Hadamard code with different carrier frequency.

Random Binary-phased Code Pulse signals (RBCP)—the transmit signals are pseudorandom binary code with same carrier frequency.

3-transmitter/3-receiver system is considered and the array structure is shown in Figure 1. The element space is selected as half wavelength (for FHCP, the element space

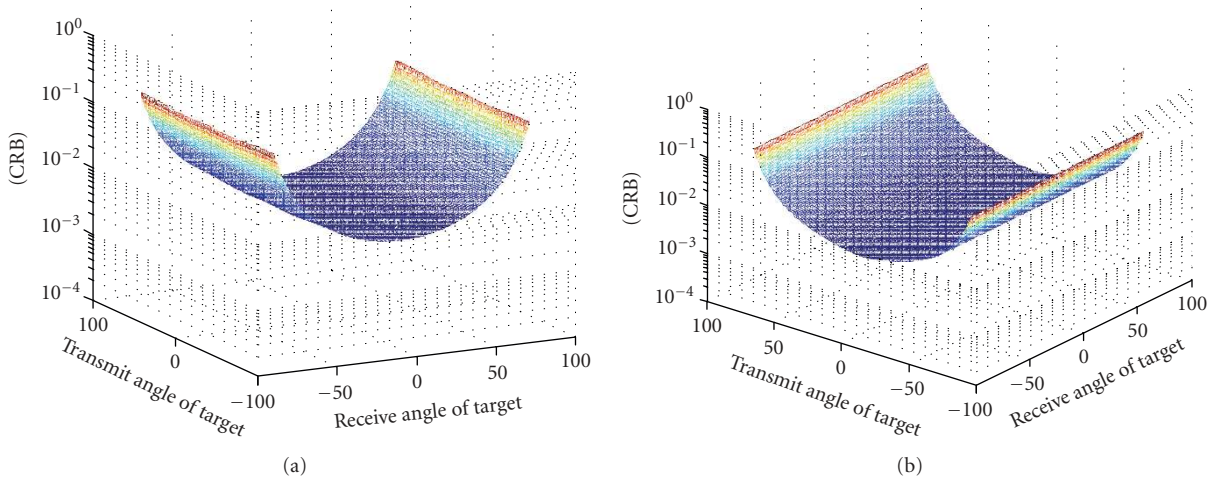

FIGURE 3: The CRB for bistatic MIMO radar, $M = N = 3$, $L = 256$, SNR = 8 dB, $\sigma_\alpha^2 = 0.1$. (a) The CRB for receive angle of range $[-80^\circ, 80^\circ]$ with transmit angle varying from -80° to 80°; (b) the CRB for transmit angle of range $[-80^\circ, 80^\circ]$ with receive angle varying from -80° to 80°.

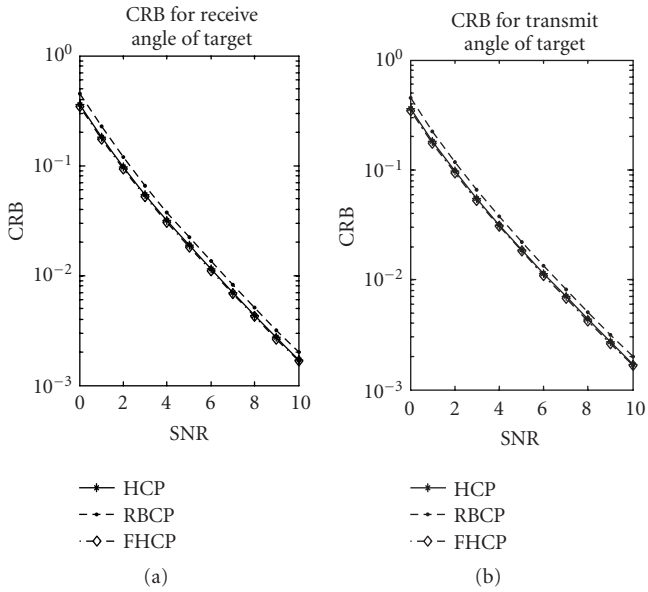

FIGURE 4: The CRB for MIMO radar of a single target with different signals; $\theta_t = 0^\circ$, $\theta_r = 0^\circ$, $\sigma_\alpha^2 = 0.1$.

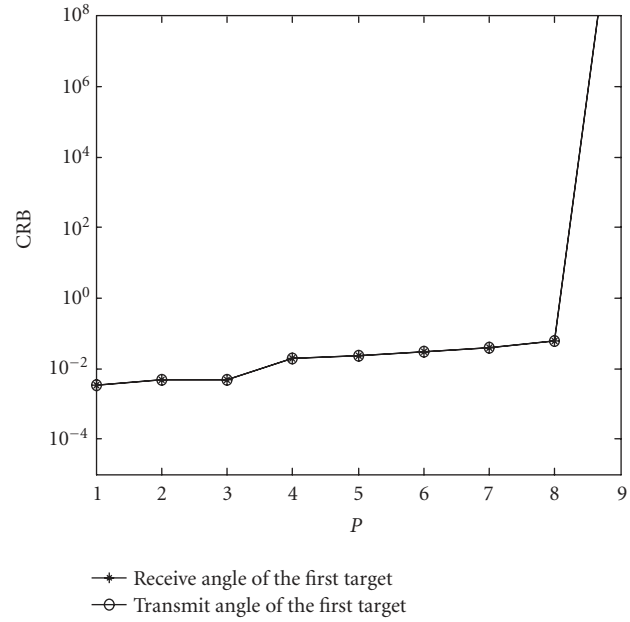

FIGURE 5: CRB of the first target located at $\theta_{r_1} = 0^\circ$, $\theta_{t_1} = 0^\circ$ versus the number of target P, SNR = 8 dB.

is the half-wavelength of the maximum carrier frequency). Figure 3 shows respectively the variation of CRB of the transmit angle and receive angle with the location of one target. The transmit signal is selected as RBCP. In Figure 3(a), we can observe that the far the target angles depart from norm of receiver, the worse the estimation performance of receive angle is. While the CRB of receive angle is kept constant with varying transmit angles. It means that the performance of receive angle is not related to transmit angle of the target. The similar conclusion for the CRB of transmit angle can also be obtained from Figure 3(b).

We compare the CRBs of location parameters for single target with different transmit signals in Figure 4. The FHCP signals, RBCP signals, and HCP signals are used, respectively. Although the correlation matrix of both FHCP signals and HCP signals is the identify matrix, it can be observed that the CRB of the former is lower than the latter. The reason is that they have different array manifolds. As the cross correlation of RBCP signals is not zero, its CRB is the worst among three transmit signals.

In Figures 5 and 6, we investigate the CRB in the case of multitarget. The transmit signal is RBCP. The CRB of Target 1 as a function of the number targets is plotted in Figure 5. The simulation parameters of the targets are given in Table 1. It is shown that the curve is almost flat when the number of the targets is less than 9. As the number of targets is nine,

Table 1: Locations of the nine targets.

Targets	1	2	3	4	5	6	7	8	9
θ_r	0	−40	−50	10	−20	40	20	50	−30
θ_t	0	−20	50	−10	−50	−40	60	30	30
σ_α^2	0.1	0.15	0.2	0.25	0.3	0.35	0.4	0.45	0.5

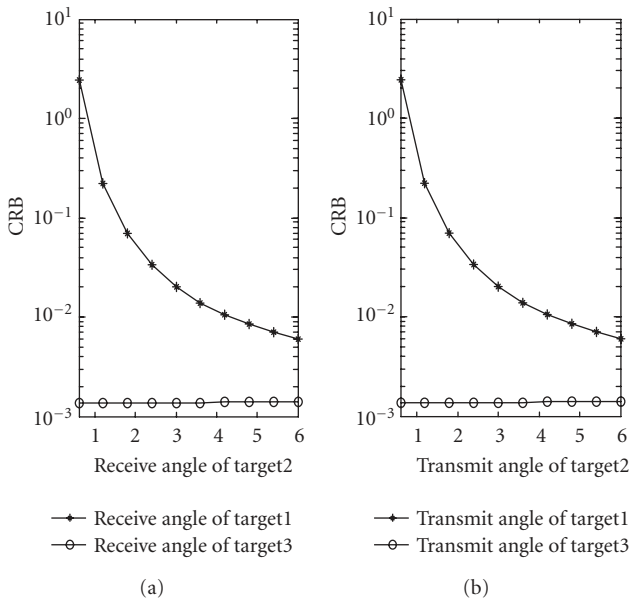

Figure 6: CRB of Target 1 and Target 3 as a function of Target 2's angles, where Target 1 locates at $\theta_{t1} = 0°$, $\theta_{r1} = 0°$, Target 3 locates at $\theta_{t3} = 50°$, $\theta_{r3} = 50°$, $\sigma_{\alpha_1}^2 = 0.7$, $\sigma_{\alpha_2}^2 = 0.75$, $\sigma_{\alpha_3}^2 = 0.8$ SNR = 8 dB.

the value of CRB is infinite. It is consistent with the result discussed previously in Section 4.1.

Figure 6 shows the interaction of the adjacent targets. Two targets are fixed at $[\theta_{t1}, \theta_{r1}] = [0°, 0°]$ (Target 1) and $[\theta_{t3}, \theta_{r3}] = [50°, 50°]$ (Target 3) with $\sigma_{\alpha_1}^2 = 0.7, \sigma_{\alpha_3}^2 = 0.8$. The location of another target (Target 2) is varying from $[\theta_{t2}, \theta_{r2}] = [0.6°, 0.6°]$ to $[6°, 6°]$ with $\sigma_{\alpha_2}^2 = 0.75$, which is very close to Target 1 and far from Target 3. It is shown that the CRB of Target 1 increases when the angles of Target 2 are close to Target 1. However, the adjacency of Target 1 and Target 2 does not almost influence the performance of Target 3.

5. SIMULATION RESULTS

In this section, we demonstrate via simulations the identification and localization performance of the scheme proposed in this paper. Three transmit antennas and three receive antennas are considered, that is, $M = N = 3$. The array structure is the same as Figure 1, and with half-wavelength space between adjacent elements used both for transmitter and receiver. Signal-to-noise ratio (SNR) is 8 dB and $L = 256$ is the number of code in one pulse period. The number of transmitted pulses is $Q = 500$.

Table 2: Locations of the six targets.

Targets	1	2	3	4	5	6
θ_t	40	−20	0	25	−50	10
θ_r	−45	−35	0	20	30	40
σ_α^2	0.6	0.65	0.7	0.75	0.8	0.85

Table 3: Locations of the eight targets.

Targets	1	2	3	4	5	6	7	8
θ_t	50	−20	−50	−10	−40	60	30	10
θ_r	−50	−40	−20	10	40	20	50	−10
σ_α^2	0.5	0.55	0.6	0.65	0.7	0.75	0.8	0.85

5.1. The influence of the transmitted signals

We demonstrate the influence of the transmitted signals with three transmitted signal cases: HCP signals, FHCP signals, and RBCP signals. The performances of these three different transmitted signal cases are plotted in Figures 7(a), 7(b), and 7(c). The target locates at $\theta_t = 0°$, $\theta_r = 0°$ with $\sigma_\alpha^2 = 0.8$. It is shown that the identification performance with HCP signals and FHCP signals is superior to the performance obtained with RBCP signals. The correlation of transmit waveform would degrade the performance.

The cases of multitarget are plotted in Figures 8(a), 8(b), and 8(c). Six targets are identified and localized effectively. It is shown that all the three signals cases can identify and locate the targets. However, HCP signals and FHCP signals have better identifibility than RBCP signals.

In Figure 9, localization and identification of eight different targets (maximum target number) are plotted in the case of three different transmitted signals. The locations of the targets are given in Table 3. It is shown that eight different targets can be identified and located in the three cases. We can see that the performance of identification in HCP signals and FHCP signals is much better than that of the case in RBCP signals. It can be observed from Figures 9(a) and 9(b) that when the target number reach the maximum identifiable number, the peak sidelobes level is much higher (approximately 10 dB) than that of the one in Figure 9(c). It can be concluded that the identification performance of FHCP signals is superior to the performance obtained by HCP signals and RBCP signals. Accordingly, the performance of target identification and location is closely related to the transmitted signals.

From Figures 7, 8, and 9, we can also observe that the targets' 2D angles can be paired automatically in our scheme. And the maximum number of targets can be identified is $(NM - 1) = (3 \times 3 - 1) = 8$, which is consistent with the conclusion in Section 4.

5.2. Identifiability of adjacent targets

In this subsection, we investigate the identifiability of two adjacent targets and its influence on another target by simulations in RBCP signals. In Figure 10(a), Target 1 is located

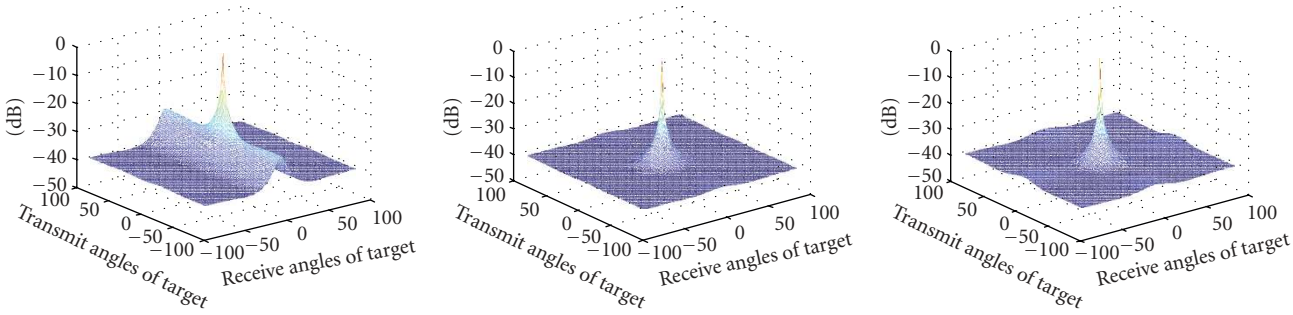

(a) RBCP signals case (b) HCP signals case (c) FHCP signals case

Figure 7: Performance of one target locates at $\theta_t = 0^\circ, \theta_r = 0^\circ, \sigma_\alpha^2 = 0.8$.

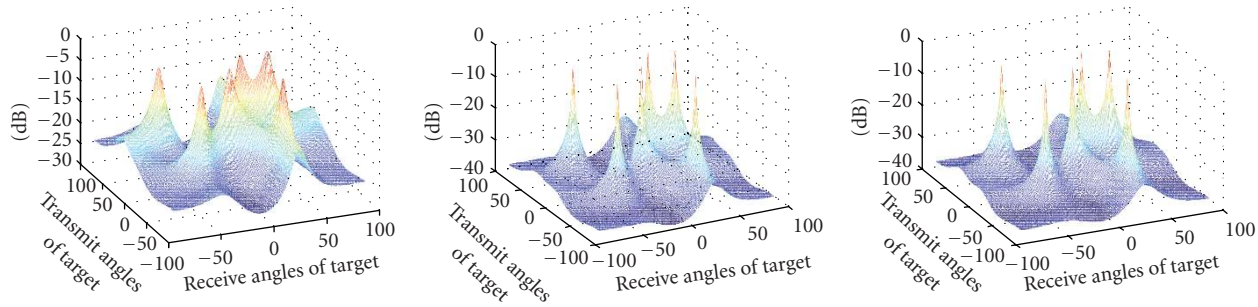

(a) RBCP signals case (b) HCP signals case (c) FHCP signals case

Figure 8: Identification and localization for six targets, SNR = 8 dB.

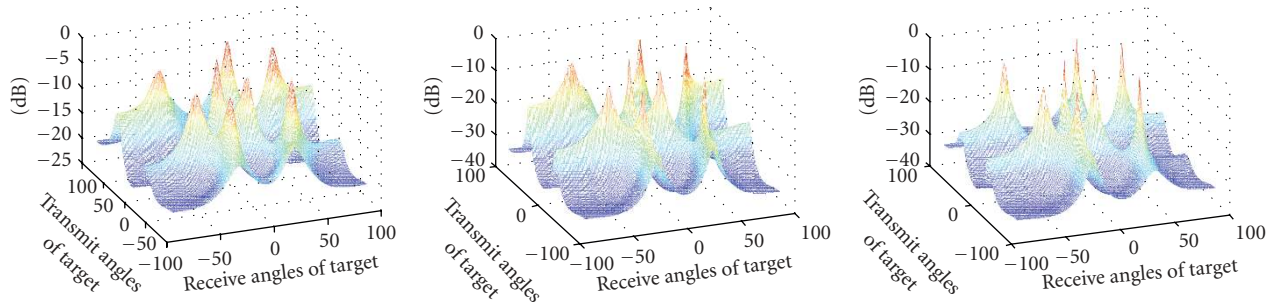

(a) RBCP signals case (b) HCP signals case (c) FHCP signals case

Figure 9: Identification and localization for six targets, SNR = 8 dB.

at $[0^\circ, 0^\circ]$ with $\sigma_{\alpha_1}^2 = 0.7$ and Target 2 is located at $[2^\circ, 2^\circ]$ with $\sigma_{\alpha_2}^2 = 0.75$. It is shown that they are too close to separate. But they do not affect the location and identification performance of Target 3 which is located at $[50^\circ, 50^\circ]$ with $\sigma_{\alpha_3}^2 = 0.8$. In Figure 10(b), the Target 2 is moved to be located at $[6^\circ, 6^\circ]$. Now it is far enough to separate Target 1 and Target 2. These simulation results are consistent with the results from the analysis of CRB in Section 4.3.

6. CONCLUSIONS

In this paper, anew scheme of multitarget resolution and localization using bistatic MIMO radar systems is presented. Multitarget can be distinguished, as well as the targets angles with respect to transmitter and receiver can be synthesized using the received signals. Accordingly, the locations of the multiple targets are obtained and spatial synchronization problem in traditional bistatic radars is avoided. The maximum number of targets that can be uniquely identified by proposed method is also analyzed. It is indicated that the product of the number of receive and transmit elements minus-one targets can be identified in the case of independently distributed targets by exploiting the spatial and temporal uncorrelation of the reflection coefficient of the targets. From Section 5, it is seen that the performance of the targets identification and localization is closely related to the form

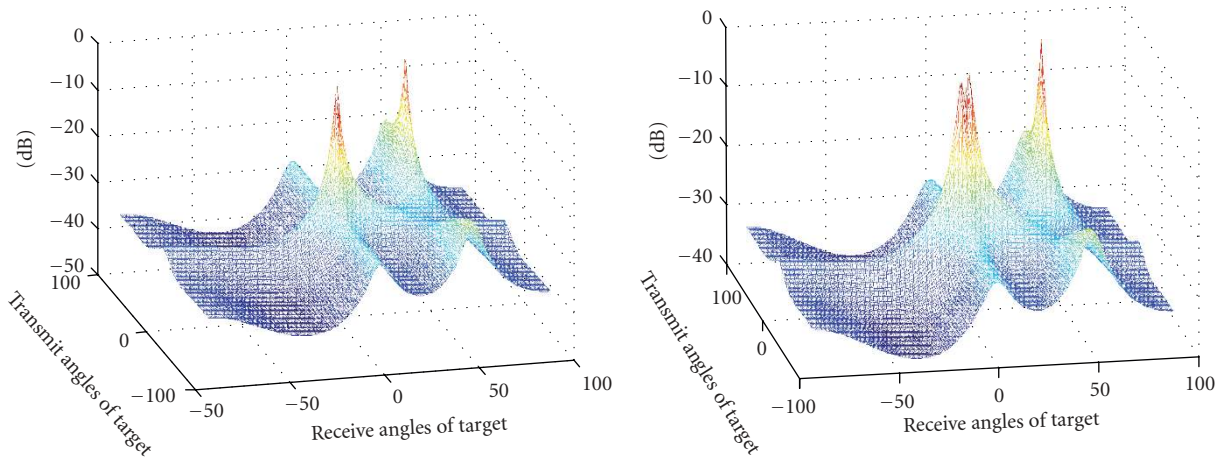

(a) Target 2 is located at $[2^\circ, 2^\circ]$

(b) Target 2 is located at $[6^\circ, 6^\circ]$

FIGURE 10: Identifiability of the adjacent targets (Target 1 $[0^\circ, 0^\circ]$; Target 3 $[50^\circ, 50^\circ]$; SNR = 8 dB, $\sigma^2_{\alpha_1} = 0.7$, $\sigma^2_{\alpha_2} = 0.75$, $\sigma^2_{\alpha_3} = 0.8$).

of the transmit signal. How to design good transmit signals for bistatic MIMO radar is the focus of our future work.

APPENDIX

A. FISHER INFORMATION MATRIX DERIVATION

In this appendix, we derive the elements of the submatrices in (9).

From (5) we can see that the observations satisfy the stochastic model $\mathbf{Y} \sim N^c(0, \mathbf{R}_\eta)$ (see [15]), where $\mathbf{R}_\eta = E\{\mathbf{Y}\mathbf{Y}^H\} \approx (1/Q)\mathbf{Y}_\eta\mathbf{Y}_\eta^H = \mathbf{K}(\boldsymbol{\theta}_r, \boldsymbol{\theta}_t)\mathbf{R}_H\mathbf{K}^H(\boldsymbol{\theta}_r, \boldsymbol{\theta}_t) + \sigma_w^2\mathbf{I}_{NM}$ is the $NM \times NM$ array data covariance matrix.

Let us consider the following matrix:

$$\mathbf{R}_H(\boldsymbol{\sigma}_\alpha) = \begin{bmatrix} \sigma^2_{\alpha_1} & & \\ & \ddots & \\ & & \sigma^2_{\alpha_p} \end{bmatrix}, \tag{A.1}$$

where $\boldsymbol{\sigma}_\alpha = [\sigma_{\alpha_1} \cdots \sigma_{\alpha_p}]^T$ is the vector of the unknown parameters which are used to parameterize the reflection coefficients covariance matrix. Thus, the $(3P+1)\times 1$ vector of unknown parameters can be written as $\boldsymbol{\xi} = [\boldsymbol{\theta}_r^T\ \boldsymbol{\theta}_t^T\ \boldsymbol{\sigma}_\alpha{}^T\ \sigma_w]^T$.

Under the previous assumptions, the Fisher information matrix (FIM) [13, Chapter 3] for the parameter vector $\boldsymbol{\xi}$ is given by

$$\mathbf{J}(\boldsymbol{\xi}) = \frac{1}{2}\mathrm{tr}\left[\mathbf{R}_\eta^{-1}(\boldsymbol{\xi})\frac{\partial \mathbf{R}_\eta(\boldsymbol{\xi})}{\partial \boldsymbol{\xi}}\mathbf{R}_\eta^{-1}(\boldsymbol{\xi})\frac{\partial \mathbf{R}_\eta(\boldsymbol{\xi})}{\partial \boldsymbol{\xi}}\right]. \tag{A.2}$$

And here we rewrite the expression of the submatrices with their elements as $\mathbf{J}_{\theta_r\theta_r} = \{J_{\theta_{r_l}\theta_{r_k}}\}_{P\times P}$, $\mathbf{J}_{\theta_r\theta_t} = \{J_{\theta_{r_l}\theta_{t_k}}\}_{P\times P}$, $\mathbf{J}_{\theta_t\theta_t} = \{J_{\theta_{t_l}\theta_{t_k}}\}_{P\times P}$, $\mathbf{J}_{\theta_r\sigma_\alpha} = \{J_{\theta_{r_l}\sigma_{\alpha_k}}\}_{P\times P}$, $\mathbf{J}_{\theta_t\sigma_\alpha} = \{J_{\theta_{t_l}\sigma_{\alpha_k}}\}_{P\times P}$, $\mathbf{J}_{\sigma_\alpha\sigma_\alpha} = \{J_{\sigma_{\alpha_l}\sigma_{\alpha_k}}\}_{P\times P}$, $\mathbf{J}_{\theta_r\sigma_w} = \{J_{\theta_{r_l}\sigma_w}\}_{P\times 1}$, $\mathbf{J}_{\theta_t\sigma_w} = \{J_{\theta_{t_l}\sigma_w}\}_{P\times 1}$, $\mathbf{J}_{\sigma_\alpha\sigma_w} = \{J_{\sigma_{\alpha_l}\sigma_w}\}_{P\times 1}$, $\mathbf{J}_{\sigma_w\sigma_w} = \{J_{\sigma_w\sigma_w}\}_{1\times 1}$, for $l, k = 1 \cdots P$.

The following derivatives are calculated firstly:

$$\begin{aligned} \frac{\partial \mathbf{K}(\theta_r, \theta_t)}{\partial \theta_{r_l}} &= \left[\mathbf{0} \cdots \frac{\partial \mathbf{k}(\theta_{r_l}, \theta_{t_l})}{\partial \theta_{r_l}} \cdots \mathbf{0}\right]_{NM\times P}, \\ \frac{\partial \mathbf{R}_H}{\partial \sigma_{\alpha_l}} &= 2\begin{bmatrix} 0 & & & \\ & \ddots & & \\ & & \sigma_{\alpha_l} & \\ & & & \ddots \\ & & & & 0 \end{bmatrix}_{P\times P}, \\ \frac{\partial(\sigma_w^2\mathbf{I}_{NM})}{\partial \sigma_w} &= 2\sigma_w\mathbf{I}_{NM} \end{aligned} \tag{A.3}$$

for $l = 1 \cdots P$.

For succinctness, we only give the detail derivation of $J_{\theta_{r_l}\theta_{r_k}}$ here:

$$\begin{aligned} J_{\theta_{r_l}\theta_{r_k}} &= \frac{1}{2}\mathbf{tr}\left\{\mathbf{R}_\eta^{-1}(\boldsymbol{\xi})\frac{\partial \mathbf{R}_\eta(\boldsymbol{\xi})}{\partial \theta_{r_l}}\mathbf{R}_\eta^{-1}(\boldsymbol{\xi})\frac{\partial \mathbf{R}_\eta(\boldsymbol{\xi})}{\partial \theta_{r_k}}\right\} \\ &= \frac{1}{2}\mathbf{tr}\left\{\mathbf{R}_\eta^{-1}(\boldsymbol{\xi})\frac{\partial(\mathbf{K}(\boldsymbol{\theta}_r, \boldsymbol{\theta}_t)\mathbf{R}_H\mathbf{K}^H(\boldsymbol{\theta}_r, \boldsymbol{\theta}_t) + \sigma_w^2\mathbf{I}_{NM})}{\partial \theta_{r_l}}\right. \\ &\qquad \left.\times \mathbf{R}_\eta^{-1}(\boldsymbol{\xi})\frac{\partial \mathbf{K}(\boldsymbol{\theta}_r, \boldsymbol{\theta}_t)\mathbf{R}_H\mathbf{K}^H(\boldsymbol{\theta}_r, \boldsymbol{\theta}_t) + \sigma_w^2\mathbf{I}_{NM}}{\partial \theta_{r_k}}\right\} \\ &= \frac{1}{2}\mathbf{tr}\left\{\mathbf{R}_\eta^{-1}(\boldsymbol{\xi})\left(\frac{\partial(\mathbf{K}(\boldsymbol{\theta}_r, \boldsymbol{\theta}_t)}{\partial \theta_{r_l}}\mathbf{R}_H\mathbf{K}^H(\boldsymbol{\theta}_r, \boldsymbol{\theta}_t)\right.\right. \\ &\qquad \left. + \mathbf{K}(\boldsymbol{\theta}_r, \boldsymbol{\theta}_t)\mathbf{R}_H\frac{\partial(\mathbf{K}^H(\boldsymbol{\theta}_r, \boldsymbol{\theta}_t)}{\partial \theta_{r_l}}\right) \\ &\qquad \times \mathbf{R}_\eta^{-1}(\boldsymbol{\xi})\left(\frac{\partial(\mathbf{K}(\boldsymbol{\theta}_r, \boldsymbol{\theta}_t)}{\partial \theta_{r_k}}\mathbf{R}_\mathbf{H}\mathbf{K}^H(\boldsymbol{\theta}_r, \boldsymbol{\theta}_t)\right. \\ &\qquad \left.\left. + \mathbf{K}(\boldsymbol{\theta}_r, \boldsymbol{\theta}_t)\mathbf{R}_H\frac{\partial(\mathbf{K}^H(\boldsymbol{\theta}_r, \boldsymbol{\theta}_t)}{\partial \theta_{r_k}}\right)\right\} \end{aligned}$$

$$= \frac{1}{2}\sigma_{\alpha_l}^2\sigma_{\alpha_k}^2 \mathbf{tr}\Big\{\mathbf{R}_\eta^{-1}(\boldsymbol{\xi})\Big(\frac{\partial \mathbf{k}(\theta_{r_l},\theta_{t_l})}{\partial\theta_{r_l}}\mathbf{k}^H(\theta_{r_l},\theta_{t_l}) + \mathbf{k}(\theta_{r_l},\theta_{t_l})\frac{\partial \mathbf{k}^H(\theta_{r_l},\theta_{t_l})}{\partial\theta_{r_l}}\Big) \times \mathbf{R}_\eta^{-1}(\boldsymbol{\xi})\Big(\frac{\partial \mathbf{k}(\theta_{r_k},\theta_{t_k})}{\partial\theta_{r_k}}\mathbf{k}^H(\theta_{r_k},\theta_{t_k}) + \mathbf{k}(\theta_{r_k},\theta_{t_k})\frac{\partial \mathbf{k}^H(\theta_{r_k},\theta_{t_k})}{\partial\theta_{r_k}}\Big)\Big\}$$

$$= \frac{1}{2}\sigma_{\alpha_l}^2\sigma_{\alpha_k}^2 \mathbf{tr}\Big\{\mathbf{R}_\eta^{-1}(\boldsymbol{\xi})\frac{\partial \mathbf{k}(\theta_{r_l},\theta_{t_l})\mathbf{k}^H(\theta_{r_l},\theta_{t_l})}{\partial\theta_{r_l}} \times \mathbf{R}_\eta^{-1}(\boldsymbol{\xi})\frac{\partial \mathbf{k}(\theta_{r_k},\theta_{t_k})\mathbf{k}^H(\theta_{r_k},\theta_{t_k})}{\partial\theta_{r_k}}\Big\}. \tag{A.4}$$

Making use of the derivation approach of (A.4) along with (A.2) and (A.3), we can also derive the other elements of the FIM as follows:

$$J_{\theta_{r_l}\theta_{t_k}} = \frac{1}{2}\sigma_{\alpha_l}^2\sigma_{\alpha_k}^2 \mathbf{tr}\Big\{\mathbf{R}_\eta^{-1}(\boldsymbol{\xi})\frac{\partial \mathbf{k}(\theta_{r_l},\theta_{t_l})\mathbf{k}^H(\theta_{r_l},\theta_{t_l})}{\partial\theta_{r_l}} \times \mathbf{R}_\eta^{-1}(\boldsymbol{\xi})\frac{\partial \mathbf{k}(\theta_{r_k},\theta_{t_k})\mathbf{k}^H(\theta_{r_k},\theta_{t_k})}{\partial\theta_{t_k}}\Big\},$$

$$J_{\theta_{t_l}\theta_{t_k}} = \frac{1}{2}\sigma_{\alpha_l}^2\sigma_{\alpha_k}^2 \mathbf{tr}\Big\{\mathbf{R}_\eta^{-1}(\boldsymbol{\xi})\frac{\partial \mathbf{k}(\theta_{r_l},\theta_{t_l})\mathbf{k}^H(\theta_{r_l},\theta_{t_l})}{\partial\theta_{t_l}} \times \mathbf{R}_\eta^{-1}(\boldsymbol{\xi})\frac{\partial \mathbf{k}(\theta_{r_k},\theta_{t_k})\mathbf{k}^H(\theta_{r_k},\theta_{t_k})}{\partial\theta_{t_k}}\Big\},$$

$$J_{\theta_{r_l}\sigma_{\alpha_k}} = \sigma_{\alpha_l}^2\sigma_{\alpha_k} \mathbf{tr}\Big\{\mathbf{R}_\eta^{-1}(\boldsymbol{\xi})\frac{\partial \mathbf{k}(\theta_{r_l},\theta_{t_l})\mathbf{k}^H(\theta_{r_l},\theta_{t_l})}{\partial\theta_{r_l}} \times \mathbf{R}_\eta^{-1}(\boldsymbol{\xi})\mathbf{k}(\theta_{r_k},\theta_{t_k})\mathbf{k}^H(\theta_{r_k},\theta_{t_k})\Big\},$$

$$J_{\theta_{t_l}\sigma_{\alpha_k}} = \sigma_{\alpha_l}^2\sigma_{\alpha_k} \mathbf{tr}\Big\{\mathbf{R}_\eta^{-1}(\boldsymbol{\xi})\frac{\partial \mathbf{k}(\theta_{r_l},\theta_{t_l})\mathbf{k}^H(\theta_{r_l},\theta_{t_l})}{\partial\theta_{t_l}} \times \mathbf{R}_\eta^{-1}(\boldsymbol{\xi})\mathbf{k}(\theta_{r_k},\theta_{t_k})\mathbf{k}^H(\theta_{r_k},\theta_{t_k})\Big\},$$

$$J_{\sigma_{\alpha_l}\sigma_{\alpha_k}} = 2\sigma_{\alpha_l}\sigma_{\alpha_k} \mathbf{tr}\{\mathbf{R}_\eta^{-1}(\boldsymbol{\xi})\mathbf{k}(\theta_{r_l},\theta_{t_l})\mathbf{k}^H(\theta_{r_l},\theta_{t_l}) \times \mathbf{R}_\eta^{-1}(\boldsymbol{\xi})\mathbf{k}(\theta_{r_k},\theta_{t_k})\mathbf{k}^H(\theta_{r_k},\theta_{t_k})\},$$

$$J_{\theta_{r_l}\sigma_w} = \sigma_{\alpha_l}^2\sigma_w \mathbf{tr}\Big\{\mathbf{R}_\eta^{-1}(\boldsymbol{\xi})\frac{\partial \mathbf{k}(\theta_{r_l},\theta_{t_l})\mathbf{k}^H(\theta_{r_l},\theta_{t_l})}{\partial\theta_{r_l}}\mathbf{R}_\eta^{-1}(\boldsymbol{\xi})\Big\},$$

$$J_{\theta_{t_l}\sigma_w} = \sigma_{\alpha_l}^2\sigma_w \mathbf{tr}\Big\{\mathbf{R}_\eta^{-1}(\boldsymbol{\xi})\frac{\partial \mathbf{k}(\theta_{r_l},\theta_{t_l})\mathbf{k}^H(\theta_{r_l},\theta_{t_l})}{\partial\theta_{t_l}}\mathbf{R}_\eta^{-1}(\boldsymbol{\xi})\Big\},$$

$$J_{\sigma_{\alpha_l}\sigma_w} = 2\sigma_{\alpha_l}\sigma_w \mathbf{tr}\{\mathbf{R}_\eta^{-1}(\boldsymbol{\xi})\mathbf{k}(\theta_{r_l},\theta_{t_l})\mathbf{k}^H(\theta_{r_l},\theta_{t_l})\mathbf{R}_\eta^{-1}(\boldsymbol{\xi})\},$$

$$J_{\sigma_w\sigma_w} = 2\sigma_w^2 \mathbf{tr}\{\mathbf{R}_\eta^{-1}(\boldsymbol{\xi})\mathbf{R}_\eta^{-1}(\boldsymbol{\xi})\}. \tag{A.5}$$

ACKNOWLEDGMENTS

This research is supported by Key Project of Ministry of Education of China under Contract no. 107102. The authors are grateful to the anonymous referees for their constructive comments and suggestions in improving the quality of this paper.

REFERENCES

[1] J. Li and P. Stoic, "MIMO radar—diversity means superiority," in *Proceedings of the 14th Adaptive Sensor Array Processing Workshop (ASAP '06)*, Lincoln Lab, Mass, USA, December 2006.

[2] E. Fishler, A. Haimovich, R. S. Blum, L. J. Cimini Jr., D. Chizhik, and R. A. Valenzuela, "Spatial diversity in radars-models and detection performance," *IEEE Transactions on Signal Processing*, vol. 54, no. 3, pp. 823–838, 2006.

[3] D. R. Fuhrmann and G. S. Antonio, "Transmit beamforming for MIMO radar systems using partial signal correlation," in *Proceedings of the 38th Asilomar Conference on Signals, Systems and Computers (ACSSC '04)*, vol. 1, pp. 295–299, Pacific Grove, Calif, USA, November 2004.

[4] L. Xu, J. Li, and P. Stoica, "Adaptive techniques for mimo radar," in *Proceedings of the 4th Workshop on Sensor Array and Multichannel Signal Processing (SAM '06)*, pp. 258–262, Waltham, Mass, USA, July 2006.

[5] I. Bekkerman and J. Tabrikian, "Target detection and localization using MIMO radars and sonars," *IEEE Transactions on Signal Processing*, vol. 54, no. 10, pp. 3873–3883, 2006.

[6] F. C. Robey, S. Coutts, D. D. Weikle, J. C. McHarg, and K. Cuomo, "MIMO radar theory and exprimental results," in *Proceedings of the 38th Asilomar Conference on Signals, Systems and Computers (ACSSC '04)*, vol. 1, pp. 300–304, Pacific Grove, Calif, USA, November 2004.

[7] E. Fishler, A. Haimovich, R. S. Blum, L. J. Cimini, D. Chizhik, and R. A. Valenzuela, "MIMO radar: an idea whose time has come," in *Proceedings of the IEEE Radar Conference*, pp. 71–78, Philadelphia, Pa, USA, April 2004.

[8] C. Baixiao, Z. Hongliang, W. Yajun, and W. Jun, "Analysis and experimental results on sparse array synthetic impulse and aperture radar," in *Proceeding of CIE International Conference Radar*, pp. 76–80, Beijing, China, October 2001.

[9] M. I. Skolnik, *Radar Handbook*, McGraw-Hill, New York, NY, USA, 1990.

[10] I. Bekkerman and J. Tabrikian, "Spatially coded signal model for active arrays," in *Proceedings of IEEE International Conference on Acoustics, Speech, and Signal Processing (ICASSP '04)*, vol. 2, pp. 209–212, Montreal, Quebec, Canada, May 2004.

[11] M. I. Skolnik, *Introduction to Radar System 3E*, McGraw-Hill, New York, NY, USA, 2001.

[12] L. Deshu, *Spatial Spectrum Estimation and Application*, University of Science and Technology of China Press, BeiJing, China, 1997.

[13] S. M. Kay, *Fundamentals of Statistical Signal Processing: Estimation Theory*, Prentice-Hall, Englewood Cliffs, NJ, USA, 1998.

[14] P. Stoica and A. Nehorai, "Performance study of conditional and unconditional direction-of-arrival estimation," *IEEE Transactions on Acoustics, Speech, and Signal Processing*, vol. 38, no. 10, pp. 1783–1795, 1990.

[15] P. Stoica, E. G. Larsson, and A. B. Gershman, "The stochastic CRB for array processing: a textbook derivation," *IEEE Signal Processing Letters*, vol. 8, no. 5, pp. 148–150, 2001.